

Multi-scale analysis of the stress state in a granular slope in transition to failure

L. Staron^{1,a}, F. Radjai², and J.-P. Vilotte³

¹ Department of Applied Mathematics and Theoretical Physics, University of Cambridge, CB3 0WA Cambridge, UK

² LMGC, CNRS-Université Montpellier II, 34095 Montpellier Cedex, France

³ Institut de Physique du Globe de Paris, 75252 Paris Cedex 05, France

Received 11 March 2005 / Received in final form 7 July 2005

Published online: 18 October 2005 – © EDP Sciences, Società Italiana di Fisica, Springer-Verlag 2005

Abstract. By means of contact dynamics simulations, we analyze the stress state in a granular bed slowly tilted toward its angle of repose. An increasingly large number of grains are overloaded in the sense that they are found to carry a stress ratio above the Coulomb yield threshold of the whole packing. Using this property, we introduce a coarse-graining length scale at which all stress ratios are below the packing yield threshold. We show that this length increases with the slope angle and jumps to a length comparable to the depth of the granular bed at an angle below the angle of repose. This transition coincides with the onset of dilation in the packing. We map this transition into a percolation transition of the overloaded grains, and discuss it in terms of long-range correlations and granular slope metastability.

PACS. 45.70.-n Granular systems – 45.70.Ht Avalanches – 81.40.Lm Deformation, plasticity, and creep

1 Introduction

The science of granular materials was initiated by Coulomb's analysis of the equilibrium and failure of a granular talus [1]. The well-known Coulomb's failure criterion was later incorporated in the framework of a rigid-plastic behaviour based on experimental testing of granular samples with homogeneous boundary conditions [2–4]. Two centuries after Coulomb, the slope failure phenomena continues to interest scientists from various fields with evident applications to geological processes and industrial handling of granular materials [5,6]. The main reason is that the phenomena involved in the evolution of a granular slope are richer than what might be expected from a mean macroscopic analysis [7–9]. On the other hand, the mechanisms leading to slope failure are not yet well understood from a grain scale standpoint [11–14].

New investigation tools, such as fine imaging techniques and discrete numerical simulations, have shown that granular media are very inhomogeneous at the grain scale, and the micro-structure, *i.e.* the organization of the grains and their contacts in space, can evolve in many different ways in response to external loading and boundary conditions [15–19]. Large fluctuations are often observed in the course of shearing [20]. Several observations suggest that surface failure may occur at slope angles well below the angle of repose [21], and that metastable states exist in the vicinity of the angle of repose [9,10].

In this context, a closer look at the micro-structure and spatio-temporal scales governing the behaviour of a granular slope cannot be avoided. The query is which internal variables or order parameters represent the evolution of a granular slope toward surface failure [22]. Even under “quasi-static” conditions, the grains in a cohesionless granular medium exhibit a high degree of mobility. Both dynamical instabilities and collective rearrangements occur frequently in response to slightest load increments [23,24,14]. This observation shows that, even in a granular medium far from macroscopic failure, the failure conditions are often fulfilled locally. Such effects may be observed by looking at grain displacements or contact forces at different scales.

In this paper, we focus on the scaling of local stresses in a two-dimensional granular bed simulated by the Contact Dynamics method. The bed is tilted slowly toward its angle of repose θ_c at which slope failure occurs. This slow gravity loading gives rise to grain rearrangements that harden the bed. Such a hardening, or plastification, process is necessary for the bed to reach its angle of repose. For example, a bed prepared initially by pouring the grains onto a rough horizontal plane, when tilted suddenly to a finite slope θ , will fail immediately. Hence, the evolution of local stress states as a function of loading is important for understanding how the failure limit is reached and in which respects it is controlled by the details of the micro-structure.

The analysis of stresses at different scales requires a quantity that plays the same role as the Cauchy

^a e-mail: L.Staron@damtp.cam.ac.uk

stress tensor in continuous media. It can be shown that the concept of “internal moment tensor”, introduced by Moreau [23], generalizes consistently the Cauchy stress tensor to discrete media and, what is more, its mechanical content with respect to Newton’s equations of motion remains the same whether applied to a single grain or to a collection of grains inside a control volume.

In the following, we first introduce the numerical procedures and the concept of stress tensor in terms of internal moments which will be used throughout the paper. We analyze the evolution of the total stress in the course of the tilting evaluating explicitly the effect of the boundary conditions. We show that the behaviour of our granular samples is consistent with a rigid plastic behaviour. Independently of the boundary conditions, no signature of the incoming instability can be identified from the total stress state. To gain further insights on the destabilisation process, we investigate the stress state from a local point of view. Analysing coarse-grained stresses as a function of the tilt angle allows us to draw an analogy with percolation. These results are discussed in terms of metastability and the emergence of long-range correlations.

2 Numerical procedures

2.1 Simulation method

For a discrete simulation of the dynamics of a collection of cohesionless rigid grains, two strategies can be adopted, differing mainly in the implementation of contact repulsion and friction. In the popular Molecular Dynamics (MD) method a repulsive potential is introduced as a function of contact interpenetration and the friction force obeys an elastic or viscous law up to a Coulomb threshold [25–27]. The equations of motion are explicitly integrated according to different classical schemes. As an interesting alternative to the MD method, the Contact Dynamics (CD) approach deals directly with infinitely stiff contact laws or, more generally “non-smooth” laws [28–33]. Hence, in contrast with MD methods, no elastic stiffness or viscous regularization of the Coulomb friction law are to be introduced at the contact level. This allows for larger time steps and thus for a substantial reduction of computational time. At the same time, no purely computational parameters are introduced, the only parameters being the inter-grain coefficient of friction μ and the normal and tangential coefficients of restitution that account for dissipation in the advent of collisions between the grains. In application to quasi-static deformations of a granular packing, one expects similar behaviors from both methods as far as large time scales (beyond the elastic response time) and plastic deformations are concerned. In the present work, we applied the CD method.

2.2 System characteristics

We consider circular grains in two dimensions, with diameters uniformly distributed in the interval $[D_{\min}, D_{\max}]$

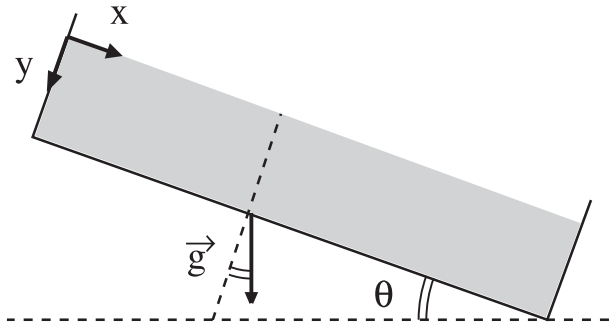


Fig. 1. Schema of the simulation: a granular bed with wall boundary conditions (WBC) is tilted in the gravity field to bring the slope of the free surface θ from originally 0 up to the angle of avalanche θ_c .

with $D_{\max}/D_{\min} = 1.5$. This slight polydispersity reduces long-range crystal-like ordering in the packing. The grains interact only through frictional cohesionless contacts with a coefficient of friction $\mu = 0.5$. The same value is used for grain-wall contacts. Moreover, we assume zero coefficients of restitution between grains. Slightly larger coefficients of restitution do not influence the mechanical behaviour in a dense granular packing where multiple contacts dissipate efficiently the kinetic energy.

The granular beds are prepared by random deposition of grains on a horizontal plane in the gravity field. The plane was made rough by sticking grains of diameter D , D being the mean diameter of the grains in the packing. Two different boundary conditions were implemented: wall boundary conditions (WBC) where the bed is confined between two vertical walls, and periodic boundary conditions (PBC) in the horizontal direction. We prepared different beds having all the same depth $H \simeq 40D$, but different lengths L . In the following, we will analyze WBC systems with $L = 100, 150, 200, 250$ and $300D$, corresponding to 4000, 6000, 8000, 10 000 and 12 000 grains respectively. The PBC system analysed is composed of 8000 grains with $L = 200$, where L refers in that case to the length of the simulation cell.

The general features of the packings are the same independently of the boundary conditions. They have a solid fraction $\rho \simeq 0.8$ and a coordination number $z \simeq 3.5$, corresponding to a random close packing. Despite the polydispersity introduced in the grain size distribution, privileged directions of contact normals at 0° , 60° and 120° with respect to the horizontal direction can still be observed.

The granular beds are tilted at a constant rotation rate $\omega = 1^\circ \text{ s}^{-1}$ in the gravity field. The slope of the free surface θ increases monotonically from $\theta = 0$ to the angle of repose $\theta = \theta_c$ (Fig. 1). At this point, the stability limit of the packing is reached and a surface flow is triggered. Analyzing a set of 50 independent simulations, we checked that both the average and local behaviours that will be discussed in this paper are highly reproducible.

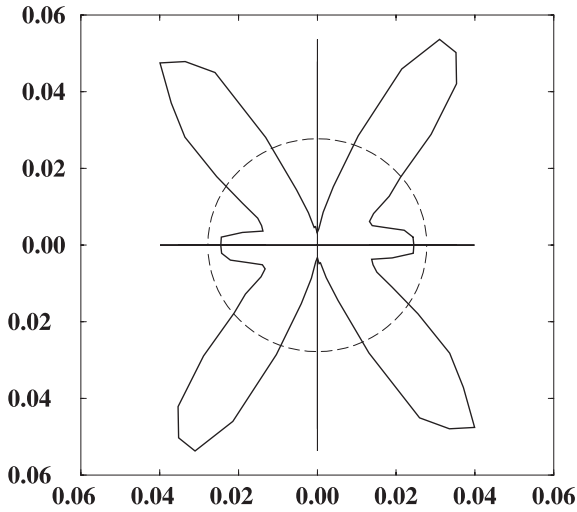


Fig. 2. Polar distribution of the contact direction in the packing in its initial state (plain line): privileged directions at 0° , 60° and 120° with are visible. The dotted line shows the corresponding uniform distribution.

3 The stress tensor

The dynamics of a granular system is naturally described in terms of grain degrees of freedom (velocities) and contact actions, including normal and tangential forces as well as contact torques (in a cohesive granular medium). This vectorial description is, however, unsuitable in a macroscopic formulation of the rheological behaviour where the material has to be described as an effective continuous medium where the stress and strain variables are stress tensors $\boldsymbol{\sigma}$ and strain tensors $\boldsymbol{\varepsilon}$ defined over representative *volumes* (in contrast to forces and velocities which act over *points*).

In principle, it is not difficult to evaluate the stress components in a control volume by simply calculating the surface density of forces applied by the grains located at one side of a surface (a line in 2D) to the grains located on the other side (Fig. 3). In this sense, the Cauchy stress tensor is as well defined as in other materials (with or without a granular structure). In the case of dilute granular materials, the convection of grain momenta is the main mechanism of stress transmission as in a classical gas. Here, we are concerned only with quasi-static deformations of a granular material for which contact actions play the main role in stress transmission. Using the above operational definition, namely calculating the surface density of forces applied by the grains on a surface, it is possible to extract an expression for the stress components σ_{ij} in terms of contact forces $\{\mathbf{f}^\alpha\}$ and the branch vectors $\boldsymbol{\ell}^\alpha$ joining the particle mass centers:

$$\sigma_{ij} = \frac{1}{V} \sum_{\alpha \in V} f_i^\alpha \ell_j^\alpha, \quad (1)$$

where V is the control volume and α denotes the contacts in V . Several authors have proposed different methods to demonstrate this or similar relations [34–36]. Such

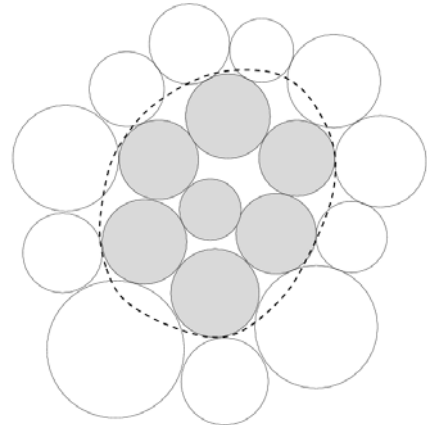


Fig. 3. The stress tensor in the volume bounded by the dashed line can be evaluated as the surface density of the forces exerted by the external grains on the grains located inside the volume.

expressions are well-defined if evaluated over a large volume containing many contacts.

There is, of course, no reason for not using the expression 1 at smaller scales down to a single grain if the volume V is properly adjusted. However, strictly speaking, the result will not be a stress tensor in the operational sense defined above. This means that the problem should be posed in reverse order: is there a quantity whose physical content remains the same whether applied to a single grain or to a collection of grains inside a control volume and that tends to the Cauchy stress tensor at large scales? Moreau showed that the concept of *internal moment tensor* fulfills these conditions [23]. For clarity, we briefly introduce this concept below.

In the framework of the virtual power formalism, a force (in the general sense) experienced by a bounded portion S of a material system is defined through the expression of the power \mathcal{P} that it develops when subjected to a virtual velocity field $\mathbf{v}(\mathbf{r})$. Let $\mathbf{v}(\mathbf{r})$ be an affine field,

$$\mathbf{v}_i(\mathbf{r}) = v_i(0) + b_{ij}r_j, \quad (2)$$

where we assume Einstein's summation rule over subscripts. By definition, the power $\mathcal{P}_{\text{int}}(\mathbf{v})$ of internal forces is linear in \mathbf{v} . This means that there exist \mathbf{R} and \mathbf{M} such that

$$\mathcal{P}_{\text{int}} = R_i v_i(0) + M_{ij} b_{ij}. \quad (3)$$

In the particular case of a rigid body motion, \mathbf{b} is antisymmetric ($b_{ij} = -b_{ji}$) and $\mathcal{P}_{\text{int}} = 0$ by virtue of Newton's third law. This implies that $\mathbf{R} = 0$ and \mathbf{M} is a symmetric tensor of rank 2 and independent of the choice of the reference frame. Following Moreau, we will refer to \mathbf{M} as the internal moment tensor of the system [23].

By definition, the internal moment tensor makes sense at all scales. In particular, we may evaluate the internal moment tensor of a grain within a granular system. The simplest example occurs when the system is in static equilibrium. In this case, the total power $\mathcal{P} = \mathcal{P}_{\text{int}} + \mathcal{P}_{\text{ext}}$, where \mathcal{P}_{ext} is the power associated with external forces, is zero independently of the choice of the virtual velocities.

If the only forces \mathbf{f}^α acting on a grain p are those exerted at its contact points \mathbf{r}^α by neighboring grains, then the internal power is $\mathcal{P}_{\text{int}}(p) = -\mathcal{P}_{\text{ext}}(p) = -\sum_{\alpha \in p} v_i(\mathbf{r}^\alpha) f_i^\alpha$ (Fig. 4). Identifying this with the general expression 3 of the internal power, we get $M_{ij}(p) = -\sum_{\alpha \in p} r_i^\alpha f_j^\alpha$. If the condition of equilibrium does not apply, the total virtual power is given by $\int \gamma(\mathbf{r}) dm$, where $\gamma(\mathbf{r})$ is the acceleration field and dm denotes the mass measure.

In the case of circular grains with moment of inertia I about the grains centers, the general expression of the internal moment tensor of a grain p becomes [23]

$$M_{ij}(p) = -\sum_{\alpha \in p} r_i^\alpha f_j^\alpha - \frac{1}{2} I \omega^2 \delta_{ij}, \quad (4)$$

where ω is the rotation velocity and δ_{ij} is the Kronecker symbol. It can be shown that the expression 4 holds also in the presence of bulk forces (gravity) acting at grain centers if the origin of coordinates for each grain is placed at its center.

The internal moment $\mathbf{M}(p_1 \cup p_2)$ of two grains p_1 and p_2 sharing a contact is the sum of their respective internal moments $\mathbf{M}(p_1)$ and $\mathbf{M}(p_2)$ because opposite reaction forces of equal magnitude act on the two grains at the *same* contact point. This additive property implies that the total internal moment $\mathbf{M}(S)$ of a system S is simply the sum of the internal moments of all grains included in S . On the other hand, if the number of grains in S is sufficiently large, it makes sense to evaluate the Cauchy stress tensor $\boldsymbol{\sigma}$ for S . Assuming the same test field as 2, the corresponding internal power by definition of $\boldsymbol{\sigma}$ is

$$\mathcal{P}_{\text{int}} = \int_V \sigma_{ij} \partial_i v_j dV. \quad (5)$$

Then, according to 3, we have

$$M_{ij}(S) = \int_V \sigma_{ij} dV = \langle \sigma_{ij} \rangle V. \quad (6)$$

This shows that the internal moment tensor of S per unit volume (\mathbf{M}/V) tends to the average Cauchy stress tensor $\langle \sigma_{ij} \rangle$ at larger scales or for an increasing number of grains contained in S .

The internal moment tensor has all the required properties for a scaling analysis of stress transmission in granular media. Conceptually, the internal moment tensor per unit volume in a discrete system plays the same role as the Cauchy stress tensor in a continuous medium. For this reason, we will refer to the internal moments of the grains as *grain stresses*. In the following, we will be more specifically interested in stress ratios, *i.e.* the ratio of the deviatoric part of grain stresses normalized by the corresponding spherical part.

4 The packing stress

In this section, we study the total stress of the granular bed as a function of the tilt angle θ . In the absence of

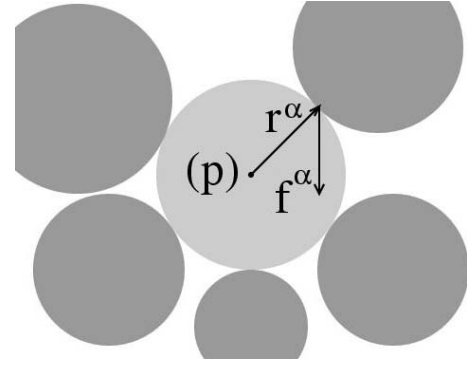


Fig. 4. Force \mathbf{f}^α applied on a grain p at the contact point \mathbf{r}^α by a neighboring grain.

plastification, *i.e.* for a rigid-plastic behaviour without rearrangements, the average stress tensor $\boldsymbol{\sigma}$ follows directly the rotation of the bed with respect to the direction of gravity (and the volume of the bed remains constant) [22]. Here, we check whether the simulations yield a picture close to this prediction in spite of rearrangement phenomena. The packing stress tensor is evaluated for the whole packing by simply adding up the grain stresses and dividing by the total volume of the packing. We consider more specifically the ratio of the normal component σ_N of the stress tensor along the direction of the free surface to the tangential component σ_T . Alternatively, we evaluate the stress ratio Γ defined as the stress deviator $Q = (\sigma_1 - \sigma_2)/2$, where σ_1 and σ_2 are the eigen values, normalized by the average stress $P = (\sigma_1 + \sigma_2)/2$:

$$\Gamma = \frac{Q}{P}. \quad (7)$$

The Coulomb criterion implies $\Gamma = \Gamma_c = \sin \theta_c$ at incipient failure, where θ_c is the angle of repose.

Figure 5 displays the evolution of the normalized shear stress σ_T/σ_N as a function of $\tan \theta$ for all samples. It is initially zero in all cases, and increases linearly with $\tan \theta$, but with different slopes depending on the length L of the granular bed. For all WBC systems, the slope is below that of the PBC system, but increases with L . The angle of repose θ_c , for which surface failure is initiated, varies between $\approx 19^\circ$ and $\approx 21^\circ$ for the WBC and the PBC systems.

In order to evaluate the influence of the walls, we consider Euler's equations for a medium in static equilibrium [37]. In a reference frame attached to the box (see Fig. 1), we have

$$\partial_x \sigma_{xx} + \partial_y \sigma_{yx} = w \sin \theta, \quad (8)$$

$$\partial_x \sigma_{xy} + \partial_y \sigma_{yy} = w \cos \theta, \quad (9)$$

where w is the specific weight of the medium. The stresses are zero at the free surface. Since the stresses are evaluated for the whole bed, we have $\sigma_N = \langle \sigma_{yy} \rangle$ and $\sigma_T = \langle \sigma_{yx} \rangle$, where $\langle \dots \rangle$ denotes averaging over the whole bed.

In the PBC case, the bed is invariant through translation along the free surface, so that $\partial_x \sigma_{xx} = 0$ and

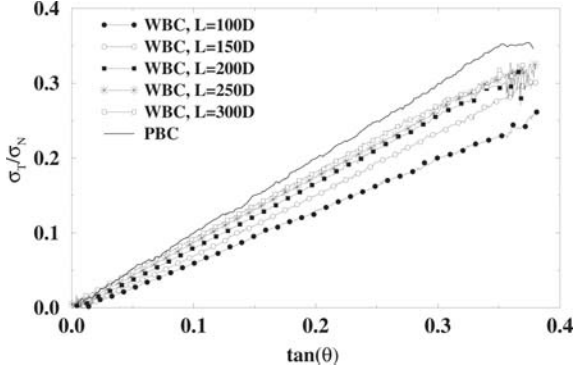


Fig. 5. Evolution of the normalized shear stress σ_T/σ_N as a function of $\tan \theta$ for all WBC and PBC systems.

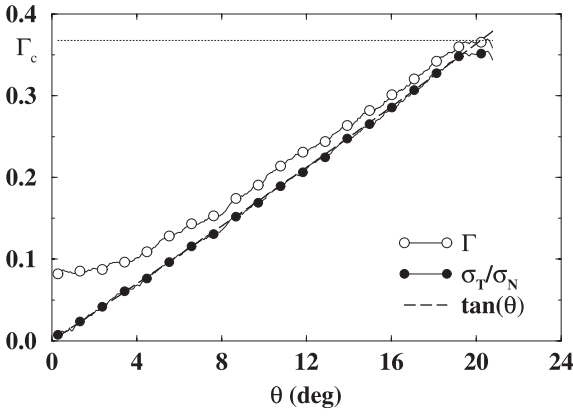


Fig. 6. Evolution of the stress ratio Γ and of the normalized shear stress σ_T/σ_N as a function of the slope angle θ for the PBC system. The dotted line corresponds to the analytical fit $\sigma_T/\sigma_N = \tan(\theta)$.

$\partial_x \sigma_{xy} = 0$. Then, Euler's equations yield $\sigma_{yx} = w \sin \theta y$ and $\sigma_{yy} = w \cos \theta y$, so that

$$\frac{\sigma_T}{\sigma_N} = \frac{\sigma_{yx}}{\sigma_{yy}} = \tan \theta. \quad (10)$$

This classical result fits perfectly the behaviour of the PBC pile (Fig. 6).

In the WBC case, the translational invariance is broken in the presence of the walls. In order to close Euler's equations, we need to make an assumption on the stress state. Our data show that the main effect of the walls is to introduce a globally nonzero gradient of the xx component along the bed (as a function of x). Figure 7 shows that this effect is localized in the vicinity of the walls as θ is increased. At the same time, the other components of stress may be considered as nearly independent of x up to wall effects.

In order to capture the influence of a stress gradient along the bed in an analytical approach, let us simply assume that σ_{xx} has a constant gradient along the bed and $\partial_x \sigma_{xy} = 0$. From Figure 7, this assumption is not exactly satisfied; yet we are concerned here only with the simplest level of description, and the influence of higher order gradients will not be evaluated. Together with equation (9), a

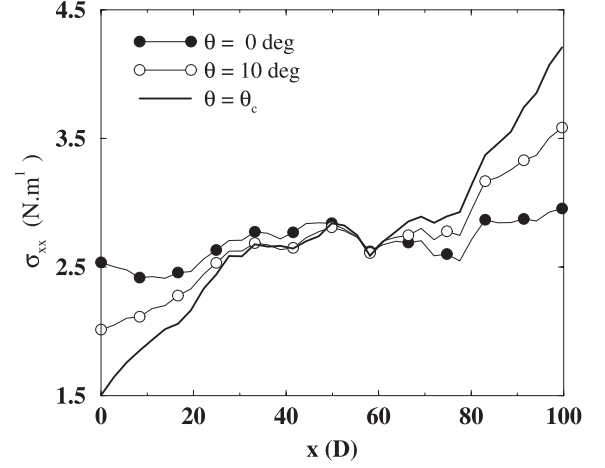


Fig. 7. Evolution of the σ_{xx} component of the stress tensor computed over successive sections of a WBC granular bed ($L = 100D$) as a function of the distance x of the section to the left wall, and for 3 values of the slope angle θ .

constant gradient implies that $\sigma_{yy} = w \cos \theta y$. We introduce two coefficients k_0 and k_L to specify the boundary values of σ_{xx} :

$$\sigma_{xx}(x=0) = k_0 w \sin \theta, \quad (11)$$

$$\sigma_{xx}(x=L) = k_L w \sin \theta. \quad (12)$$

These two coefficients might depend on θ . In the PBC case, we have $k_0 = k_L = 1$, and their values in the presence of the walls reflect small perturbation to translational invariance. We naturally expect that the normal stress $\sigma_{xx}(x=L)$ on the lower wall is larger than the normal stress $\sigma_{xx}(x=0)$ on the upper wall when $\theta > 0$, so that $k_L > k_0$. Given these boundary conditions, and since σ_{xx} is assumed to have a constant gradient, we have

$$\sigma_{xx} = \left\{ k_0 + \frac{x}{L}(k_L - k_0) \right\} w \sin \theta y. \quad (13)$$

Then, from equation (8) we get

$$\frac{\sigma_T}{\sigma_N} = \tan \theta \left\{ 1 - \frac{k_L - k_0}{3} \frac{H}{L} \right\}. \quad (14)$$

This equation, with basically one fitting parameter $k_L - k_0$, captures the features observed in Figure 5. In particular, since $k_L - k_0 > 0$, the ratio increases with L and it tends to $\tan \theta$ as $H/L \rightarrow 0$. Figure 8 shows the variation of $(\sigma_T/\sigma_N)/\tan \theta$ for $\theta = \theta_c$ as a function of L from the numerical data, together with the analytical form (14). The latter reasonably fits the data with $k_L - k_0 \simeq 2.5$, although a slight deviation can be observed.

The evolution of the total stress, when explicitly accounting for the walls effects, is consistent with a rigid plastic behaviour. Independently of the boundary conditions, no signature of the incoming instability can be identified from the total stress state. To gain further insights on the destabilisation process, we now investigate how the macroscopic stress state builds up when analysing stress

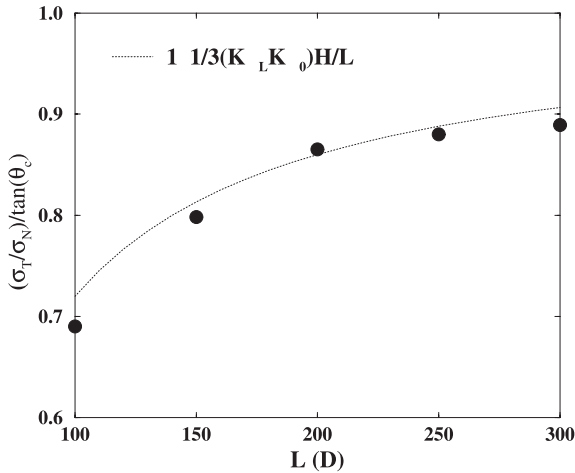


Fig. 8. Ratio $(\sigma_T/\sigma_N)/\tan\theta$ for $\theta = \theta_c$ as a function of L for the WBC system (black circles). The dotted line represents the analytical form given by equation (14), with $k_L - k_0 \simeq 2.5$.

from a local point of view. In the forthcoming sections, we focus on the PBC system; all the observed features are robust with the boundary conditions.

5 Local stresses

5.1 Grain stress distributions

According to the definition of grain stresses (4), one can attribute to each grain a stress deviator q and a mean stress p . Figure 9 displays the probability density function (pdf) $P(\gamma)$ of the grain stress ratios $\gamma = q/p$ for $\theta = 0$, $\theta = 10^\circ$ and $\theta = 15^\circ$ in the PBC system. These distributions are wide and cover all possible values of γ in the range $[0, 1]$. We define the macroscopic limit stress ratio $\Gamma_c = \Gamma(\theta_c)$ reached by the granular bed at stability limit (Fig. 6). We observe that even at low slope angles, a large fraction of the grains has a stress ratio γ above the limit stress ratio Γ_c (represented by a vertical line in Fig. 9). The initial fraction (at $\theta = 0$) of these “overloaded” grains is about 30%. Since the largest permissible grain stress ratios are controlled by the immediate environment of each grain, they can indeed overpass the macroscopic threshold Γ_c . This fraction grows with θ and eventually reaches $\simeq 60\%$ at θ_c , as shown in Figure 10.

Figure 11 shows successive snapshots of the packing (in the frame attached to the simulation box) for $\theta = 0, 5^\circ, 10^\circ, 15^\circ$ and $\theta = \theta_c$. Overloaded grains only are represented in black. This evolution shows well-defined clusters of overloaded grains building up while the pile gets closer to stability limit. For comparison, Figure 12 shows the clustering obtained from a stochastic process in the same pile, where black grains represent 60% of the total number of grains. This snapshot should thus be compared with Figure 11 for $\theta = \theta_c$, for which overloaded grains are in a proportion of 60%. We can see that no obvious clustering can be seen in Figure 12, by contrast with Figure 11. The existence of clusters of overloaded grains shown in

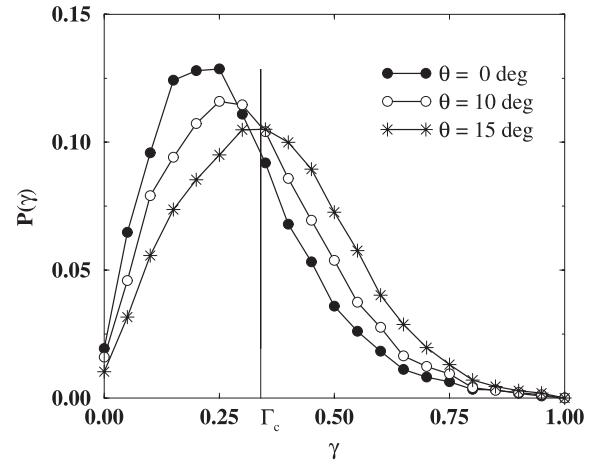


Fig. 9. Probability density function (pdf) $P(\gamma)$ of the grain stress ratios $\gamma = q/p$ for $\theta = 0$, $\theta = 10^\circ$ and $\theta = 15^\circ$ in the PBC system. The vertical line shows the value of the critical stress ratio Γ_c of the packing.

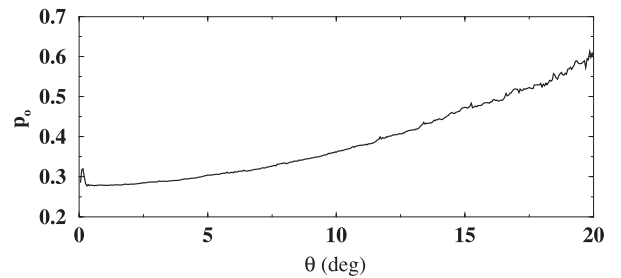


Fig. 10. Evolution of the fraction p_o of overloaded grains in the PBC system as a function of the slope angle θ .

Figure 11 and their size evolution when $\theta \rightarrow \theta_c$ suggest the existence of spatial correlations evolving in the course of time, and is strongly reminiscent of a percolation process. Indeed, these clusters eventually coalesce to form a connex network spanning the packing from top to bottom. This questions the apparition of a volume over which the macroscopic failure criteria $\Gamma = \Gamma_c$ would apply, and thus would announce the proximity of the stability limit, or at least the probability of a local failure. The simple analysis of the clusters shown in Figure 11 is not sufficient to answer this question: indeed, even though the grains all satisfy $\gamma \geq \Gamma_c$, nothing is said on the local orientation of the stress. We thus need to analyse the evolution of the stress state at the scale of the clusters, namely at the meso-scale, and no longer at the scale of the grains.

5.2 Coarse-graining stress

We want to characterise the typical size of the volumes over which the stress ratio overcomes the macroscopic limit Γ_c . To do so, we consider circular neighbourhoods of diameter ℓ centered on overloaded grains, with ℓ ranging from the mean size of the grains to the size of the system (Fig. 13). For each overloaded grain, the stress ratio γ_ℓ is computed over the circular neighbourhood of diameter

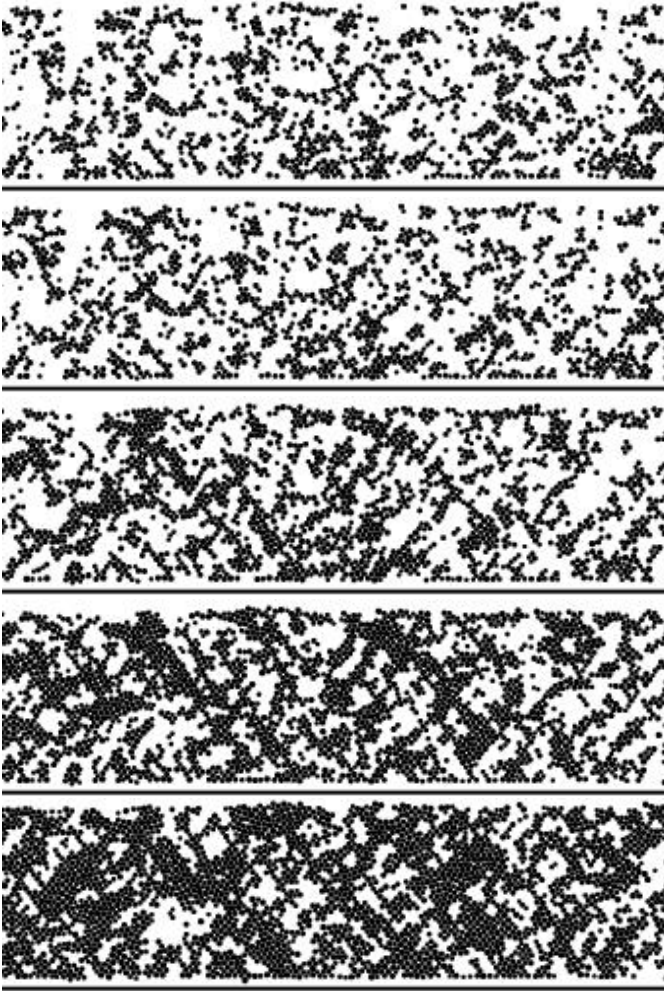


Fig. 11. Maps of the overloaded grains (in black) for successive values of θ . From top to bottom, $\theta = 0$, $\theta = 5^\circ$, $\theta = 10^\circ$, $\theta = 15^\circ$ and $\theta = \theta_c$. They form growing clusters which eventually span the packing from top to bottom.

ℓ . Thereby we determine, for each grain and at different slope angles θ , the length ℓ_c for which $\gamma_{\ell_c} = \Gamma_c$. We are thus able to plot the evolution of the maximum value ℓ_c^{\max} and the mean value $\ell_c^{\text{mean}} = (1/N_o) \sum_{N_o} \ell_c$ as a function of θ (where N_o is the total number of overloaded grains).

The length ℓ_c measures the size of volumes in the state Γ_c , in which the grains stresses lead to a critical macroscopic state when added up. The plots of ℓ_c^{mean} and ℓ_c^{\max} as a function of θ are displayed in Figure 14. The mean radius ℓ_c^{mean} first increases very slowly from $4D$ to $5D$. Then, from $\theta = 15^\circ$ onward, it increases rapidly to $\simeq 7D$. At the same angle $\theta = 15^\circ$, denoted θ_d in all the following, we observe a spectacular transition in the evolution of ℓ_c^{\max} . The latter first increases continuously from $5D$ at $\theta = 0$ to $15D$ at $\theta = \theta_d$. Here, a sudden jump brings ℓ_c^{\max} from $15D$ to $30D$. The cutoff at $30D$ is imposed by data processing for the evaluation of ℓ_c . However, this value is close enough to the depth $H = 40D$ of the granular bed to be interpreted as corresponding to the system size. The behaviour of ℓ_c^{\max} is very robust from one realisation to

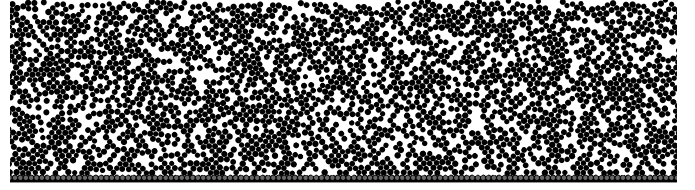


Fig. 12. Snapshot of the pile showing the pattern induced by a stochastic process based on the random distribution of grain size. Black grains represent grains with a radius greater than $0.85D$ so that they represent 60% of the total number of grains. Their distribution can be compared with Figure 11 for $\theta = \theta_c$. The scale is the same as in Figure 11.

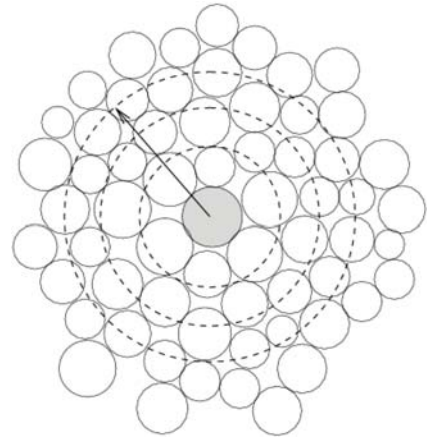


Fig. 13. Successive circular neighborhoods of diameter ℓ centered on one overloaded grain (in gray). The stress ratios γ_ℓ of the grain are computed over these neighborhoods as a function of ℓ .

another as well as with boundary conditions. Slight variations only are observed in the value of the angle θ_d at which the transition occurs.

As previously in Figure 11, it is interesting to map the growth of ℓ_c^{\max} and its nearly discontinuous change at $\theta = \theta_d$ into a percolation process. In this picture, the transition at $\theta = \theta_d$ is a percolation transition for which the largest cluster size diverges, spanning the whole system. The fraction of overloaded grains at the transition is $p_o = 0.48$ (Fig. 10). Interestingly, this proportion is close to the percolation threshold for randomly built-up structures of non-overlapping particles in two dimensions [38–40].

6 Transition to coherent shearing

The evolution of the packing stress ratio Γ with θ (Fig. 6) carries no apparent signature of a discontinuous transition at θ_d . Irrespective of boundary conditions and for different values of the aspect ratio H/L , the packing stress follows closely the loading direction up to slope failure. Such a signature should thus appear in the volume-change behaviour of the packing. Figure 15 shows the volumetric

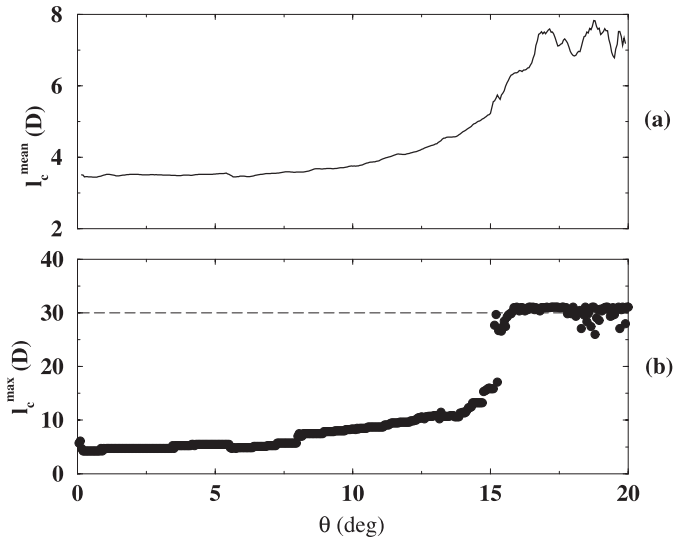


Fig. 14. Evolution of l_c^{mean} (a) and l_c^{max} (b) as a function of θ (see text for definitions).

strain $\varepsilon_V = (V - V_0)/V_0$, where V_0 is the initial volume, as a function of θ in the PBC system. We see that the volume first decreases (negative values of ε_V) with θ . Then, precisely at $\theta = \theta_d$, for which transition in the stress state is observed (Fig. 14), this contractant behaviour transforms into a dilatant behaviour, with the volume increasing up to slope failure.

Since packing dilation may occur only as a consequence of shearing, the transition to dilation at θ_d can be interpreted as the onset of a stable shear mode in the packing. Before transition, the particle rearrangements occur in a diffuse and incoherent manner in the whole packing: in the presence of geometrical disorder and gravity, each grain tends to occupy a more stable position. Such rearrangements take place mostly in a collective way, but in small volumes compared to the size of the system [14]. They do not disturb the overall stability of the slope, neither at the free surface nor in the bulk.

This behaviour is reminiscent of the contractant behaviour observed in the first stages of a shear test performed on soil samples [41]. The extent of volume reduction depends on the initial solid fraction of the packing. A transition to dilatancy happens if the initial solid fraction is above the “critical state” solid fraction, *i.e.* the solid fraction corresponding to a state reached after long enough monotonous shearing [3]. This is an interesting analogy although in a granular slope the gravity behaves as a bulk force, in contrast to shear testing conditions where the largest stresses are exerted at the wall boundaries.

7 Discussion and conclusion

7.1 Summary

We performed numerical simulations of granular slopes composed of rigid disks and tilted in the gravity field

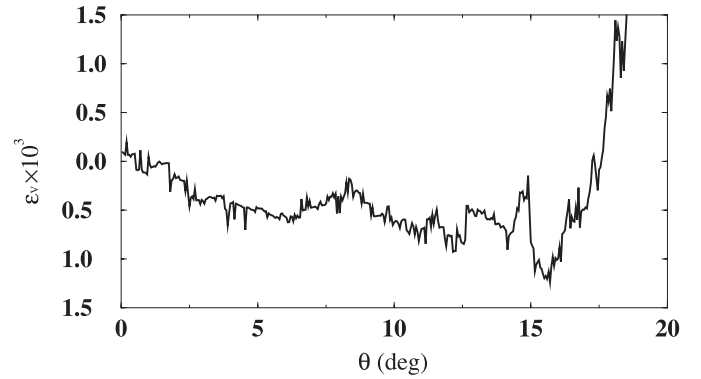


Fig. 15. Evolution of the volumetric strain $\varepsilon_V = (V - V_0)/V_0$, V_0 being the initial volume, as a function of θ in the PBC system.

towards stability limit using the Contact Dynamics method. We showed that a global stress analysis in terms of Euler’s equations for periodic boundary conditions along the free surface fits the simulation data. The influence of side-walls was evaluated as a function of the total length L of the free surface. We showed that the evolution of the total stress is consistent with a rigid plastic behaviour. Independently of the boundary conditions, no signature of the incoming instability can be identified from the total stress state. To gain further insights on the destabilisation process, we investigated how the macroscopic stress state builds up when analysing stress from a local point of view. The local stresses are described in terms of internal moments which allow for an additive coarse-graining of stresses. We observe a wide distribution of grain stress ratios involving a significant fraction of the so-called “overloaded” grains, for which the stress ratio γ is above the macroscopic limit stress ratio Γ_c , corresponding to the Coulomb yield threshold for the whole packing. On the ground of the spatial distribution of the overloaded grains, showing clustering, we define a characteristic length l_c as the size of a control volume where the stress ratio is just equal to the limit stress ratio Γ_c . The largest length l_c^{max} is a coarse-graining length evolving in the course of time. We found that l_c^{max} increases as the bed is slowly tilted toward its angle of repose θ_c ; at an angle θ_d below θ_c , l_c^{max} undergoes a sudden jump to a length comparable to the depth of the bed. An analogy between the evolution of the local stresses and a percolation process is drawn. In this picture, the discontinuous increase of the coarse-graining length l_c^{max} at θ_d corresponds to a percolation transition. Remarkably, this transition coincides with the onset of dilation in the packing.

7.2 Discussion

The above results reveal an unexpectedly rich scaling of stresses in a granular bed in the vicinity of slope failure. In particular, when interpreted in terms of a percolation process, they are consistent with the advent of a “phase transition” at θ_d . This transition coincides with the

apparition of a volume of size comparable to the system size, and where the limit stress state corresponding to stability limit is reached. In addition, it coincides with the apparition of coherent dilatant shearing. This transition is all the more interesting that it occurs far enough from the angle of repose θ_c to be considered as a strong precursor of the incoming surface instability.

Although the transition angle θ_d appears here in the course of a “quasi-static” evolution of the slope, it is still tempting to identify θ_d with the *dynamic* angle of repose, *i.e.* the angle reached when the slope comes to rest after failure. This is an appealing interpretation in that it relates the dynamic angle of repose to a *static* property of the packing. The order parameter in this description is the fraction of overloaded grains. Further simulations are necessary to check this conjecture, but let us simply consider here an argument in this direction.

The transition observed in the evolution of the local stress should be discussed in the light of experimental results showing the increase of the sensitivity of the slope to perturbation in an interval of slope angle similar to our interval $\delta\theta = \theta_c - \theta_d$ [9,10]. In other words, the interval of slope angle $[\theta_d, \theta_c]$ coincides with a metastable state. It is tempting to relate this metastability to the apparition of long-range correlations in the system, which may help propagating an existing perturbation to the totality of the packing. This is a possible interpretation of the existence of these large clusters of overloading grains, leading to the appearance of volumes where the critical stress state Γ_c is reached. Indeed, one can expect any perturbation to degenerate in these volumes once they are of a large enough size for the macroscopic failure criteria to make sense. Earlier work on the mobilisation of friction also hinted at the apparition of large-scale correlations in the system [14]. However, we did not observe any clear transition at θ_d when computing the pair correlation functions of contact forces and grain stresses. In this case, the correlation length remains of the order of a few grain diameters all along the simulation. Further analysis, including the grains displacements, have thus to be conducted to conclude to the existence of large-scale correlations.

The dilation of the bed provides another interesting insight into the behaviour of a granular bed in the metastable range. The avalanche can not occur unless the bed dilates. Since the bed begins to dilate at θ_d , the angle $\theta_c - \theta_d$ should be interpreted as the “dilation angle” of the granular material when plastified as a result of rearrangements induced by the rotation of the bed [37]. Hence, in a macroscopic approach, the static angle of repose θ_c and the transition angle θ_d , interpreted as the dynamic angle of repose, may be described in terms of the Coulomb yield criterion and the dilation angle, respectively.

We acknowledge very fruitful discussions with J.-J. Moreau. This work was supported by the Marie Curie European Fellowship FP6 Program Grant # 500511.

References

1. C.A. Coulomb, Acad. Roy. Sci. Math. Phys. **7**, 343 (1773)
2. D.C. Drucker, J. Appl. Mech. **21**, 71–74 (1954)
3. D.M. Wood, *Soil behaviour and critical state soil mechanics* (Cambridge University Press, Cambridge, 1990)
4. M. Oda, K. Iwashita, eds., *Mechanics of Granular Materials* (A.A. Balkema, Rotterdam, 1999)
5. H.M. Jaeger, S. Nagel, Rev. Mod. Phys. **68**, 1259 (1996)
6. P.-G. de Gennes, Rev. Mod. Phys. **71**, S374 (1999)
7. H.M. Jaeger, C. Liu, S.R. Nagel, Phys. Rev. Lett. **62**, 40 (1989)
8. F. Darve, F. Laouafa, Mech. Cohesive-Frictional Mat. **5**, 627 (2000)
9. A. Daerr, S. Douady, Nature **399**, 241 (1999)
10. S. Deboeuf, E.M. Bertin, E. Lajeunesse, O. Dauchot, Eur. Phys. J. B **36**, 105 (2003)
11. L. Quartier, B. Andreotti, S. Douady, A. Daerr, Phys. Rev. E **62**, 8299 (2000)
12. J.J. Alonso, J.-P. Hovi, H.J. Herrmann, Phys. Rev. E **58**, 672 (1998)
13. A. Lemaître, Phys. Rev. Lett. **89**, 064303 (2002)
14. L. Staron, J.-P. Vilotte, F. Radjai, Phys. Rev. Lett. **89**, 204302 (2002)
15. M. Oda, Soils Found. **12**, 17 (1972)
16. M. Oda, J. Koshini, S. Nemat-Nasser, Geotechnique **30**, 479 (1980)
17. L. Rothenburg, R.J. Bathurst, Geotechnique **39**, 601 (1989)
18. B. Cambou, in *Powders and Grains 93*, edited by C. Thornton (A.A. Balkema, Amsterdam, 1993), p. 73
19. F. Radjai, in *Physics of dry granular media – NATO ASI Series E350*, edited by H.J. Herrmann, J.-P. Hovi, S. Luding (Kluwer Academic Publishers, Dordrecht, 1998), p. 305
20. D. Howell, R.P. Berhinger, C. Veje, Phys. Rev. Lett. **82**, 5241 (1999)
21. F. Darve, F. Laouafa, in *Numerical Models in Geomaterials*, edited by Prande, Pietruszczak, Schweiger (Balkema, Rotterdam, 1999), p. 85
22. S. Roux, F. Radjai, in *Mechanics for a New Millennium*, edited by H. Aref, J. Philips (Kluwer Acad. Pub., Netherlands, 2001), p. 181
23. J.-J. Moreau, in *Friction, Arching, Contact Dynamics* (World Scientific, Singapore, 1997), p. 233
24. F. Radjai, S. Roux, Phys. Rev. Lett. **89**, 064302 (2002)
25. P.A. Cundall, O.D.L. Stack, Geotechnique **29**, 47 (1979)
26. H.J. Herrmann, Physica A **191**, 263 (1992)
27. S. Luding, in *Physics of dry granular media – NATO ASI Series E350*, edited by H.J. Herrmann, J.-P. Hovi, S. Luding (Kluwer Academic Publishers, Dordrecht, 1998), p. 285
28. J.-J. Moreau, in *Nonsmooth mechanics and applications*, edited by J. Moreau, P. Panagiotopoulos (Springer Verlag, 1988)
29. M. Jean, J.-J. Moreau, in *Proc. of Contact Mech. Int. Symp.*, edited by A. Curnier (1992a), p. 31

30. M. Jean, J.-J. Moreau, in *Proceedings of Contact Mechanics International Symposium* (Presses Polytechniques et Universitaires Romandes, Lausanne, Switzerland, 1992b), p. 31
31. J.-J. Moreau, *Europ. J. Mech. A/Solids* **Supp.**(4), 93 (1994)
32. M. Jean, *Frictional contact in rigid or deformable bodies: numerical simulation of geomaterials* (A.P.S. Salvadurai J.M. Boulon, Elsevier Science Publisher, Amsterdam, 1995), p. 463
33. F. Radjai, D.E. Wolf, M. Jean, J.-J. Moreau, *Phys. Rev. Lett.* **90**, 61 (1998)
34. J. Christoffersen, M.M. Mehrabadi, S. Nemat-Nasser, *J. Appl. Mech.* **48**, 339 (1981)
35. N.P. Kruyt, L. Rothenburg, *J. App. Mech.* **118**, 706 (1996)
36. J.D. Goddard, *Physics of dry granular media* (Kluwer Academic Publishers, 1998), Chap. Continuum modeling of granular assemblies
37. R.M. Nedderman, *Statics and kinematics of granular materials* (Cambridge Univ. Press, Cambridge, 1992)
38. H.L. Frisch, E. Sonnenblick, V.A. Vyssotsky, J.M. Hammersley, *Phys. Rev.* **124**, 1021 (1961)
39. M.F. Sykes, J.W. Essam, *Phys. Rev.* **133**, A310 (1964)
40. H. Scher, R. Zallen, *J. Chem. Phys.* **53**, 3759 (1970)
41. P.-Y. Hicher, in *Behaviour of Granular Materials* (Springer, Wien, 2000), p. 1